ination of periods of low magnetic field strength, during which the radial Lorentz force is insufficient to retard the radial diffusion of ions and electrons in the plasma. In addition to increasing analyte line-to-background intensity ratios, the hotter plasma core associated with the unidirectional discharge should be useful in the analysis of refractory solid powder samples. Preliminary studies[14] have indicated that the graphite vapor theta-pinch plasma may be useful for the direct analysis of solid powders.

The principal problem associated with the present unidirectional discharge system is the limitation to operation at 6 kV or less. This situation should be corrected by the use of fast-recovery diodes. Alternatively, a discharge circuit based on a distributed-element LC transmission line should be capable of producing unidirectional, nearly square-wave current pulses without the use of a diode shunt. A low-voltage prototype circuit has produced very encouraging results.

1. S. R. Goode and D. T. Pipes, Spectrochim. Acta **36B**, 925 (1981).
2. G. J. Kamla and A. Scheeline, Anal. Chem. **58**, 923 (1986).
3. G. J. Kamla and A. Scheeline, Anal. Chem. **58**, 932 (1986).
4. R. J. Klueppel and J. P. Walters, Spectrochim. Acta **35B**, 431 (1980).
5. V. Majidi and D. M. Coleman, Appl. Spectrosc. **41**, 200 (1987).
6. D. Albers, E. Johnson, M. Tisack, and R. Sacks, Appl. Spectrosc. **40**, 60 (1986).
7. D. Albers and R. Sacks, Spectrochim. Acta **41B**, 968 (1986).
8. D. Albers, M. Tisack, and R. Sacks, Appl. Spectrosc. **41**, 131 (1987).
9. D. Albers and R. Sacks, Anal. Chem. **59**, 593 (1987).
10. K. Trivedi, S. Tanguay, M. Matties, and R. Sacks, Appl. Spectrosc. **41**, 833 (1987).
11. J. A. Thornton and A. S. Penfold, in *Thin Film Processes*, J. L. Vossen and W. Kern, Eds. (Academic Press, New York, 1978), Chap. 2, p. 75.
12. K. I. Kirov, N. A. Ivanov, E. D. Atanasova, and G. M. Minchev, Vacuum **26**, 237 (1976).
13. E. T. Johnson and R. D. Sacks, Anal. Chem. **59**, 2170 (1987).
14. E. T. Johnson and R. D. Sacks, Anal. Chem. **59**, 2176 (1987).
15. J. P. Walters, Anal. Chem. **40**, 1672 (1968).
16. D. M. Coleman and J. P. Walters, Spectrochim. Acta **31B**, 547 (1976).
17. F. F. Chen, *Introduction to Plasma Physics* (Plenum Press, New York, 1974).
18. T. J. M. Boyd and J. J. Sanderson, *Plasma Dynamics* (Barnes and Noble, New York, 1969).
19. R. J. Commisso and H. R. Griem, Phys. Fluids **20**, 44 (1977).
20. K. F. McKenna and T. M. York, Phys. Fluids **20**, 1556 (1977).
21. S. Y. Suh, R. J. Collins, and R. D. Sacks, Appl. Spectrosc. **35**, 42 (1981).

UV Raman Excitation Profiles of Imidazole, Imidazolium, and Water

SANFORD A. ASHER* and JAMES L. MURTAUGH

Department of Chemistry, University of Pittsburgh, Pittsburgh, Pennsylvania 15260

Preresonance absolute differential Raman cross sections have been measured between 217 and 600 nm for the symmetric ring mode vibrations of imidazole and imidazolium and for the 1645-cm^{-1} bending vibration of water. For imidazole and imidazolium the Raman intensities observed with visible wavelength excitation derive mainly from states in the far-UV. The two 190-210 nm $\pi \rightarrow \pi^*$ transitions in these species dominate the Raman intensities only for excitation below 300 nm. Both $\pi \rightarrow \pi^*$ transitions appear to contribute equally to preresonance enhancement. The data project that selective imidazole ring enhancement from histidine residues in proteins will require excitation below 210 nm. The intensities of the 1645-cm^{-1} bending vibration of water derive from states in the far-UV. The Raman cross section of this vibration increases only slightly faster than the scattered frequency to the fourth power. This Raman band can now be used as an internal intensity standard for aqueous Raman studies. Preresonance Raman enhancement dominated by transitions which occur at extraordinarily high energies have now been observed for water, acetonitrile, acetone, sulfate, and perchlorate. This behavior may result because molecular valence transitions in the vacuum UV spectral region of condensed phase samples are strongly mixed with ionizing, charge transfer, and Rydberg transitions and have *no* separate and discrete existence.

Index Headings: **Fluorescence; Instrumentation, Raman; YAG eximer lasers; Light scattering; Luminescence; Optics; Raman spectroscopy; Spectroscopic techniques; Time-resolved spectroscopy; UV-visible spectroscopy.**

Received 6 June 1987.

* Author to whom correspondence should be sent.

INTRODUCTION

The recent extension of Raman spectral measurements into the UV spectral region has resulted in a number of Raman excitation profile studies of small molecules such as acetamide, *N*-methylacetamide,[1,2] acetonitrile, sulfate, nitrate, and perchlorate[3] and larger aromatic molecules such as benzene,[4-7] substituted benezene derivatives,[8,9] imidazole, imidazolium,[10] and aromatic amino acids.[10-15] Other studies examined nucleic acids,[16-19] proteins,[15,20-22] and polycyclic aromatic hydrocarbons such as pyrene.[23-25] The motivations for these studies include establishing the principles of resonance enhancement,[1-10] exploring excited states of these species, and demonstrating the analytical utility of resonance Raman scattering for studying aromatics in complex systems such as aromatic amino acids in proteins and polycyclic aromatic hydrocarbons in coal liquid samples.[10-15,23-26]

Often resonance Raman enhancements of six to seven orders of magnitude are observed with UV excitation, in comparison to results from visible wavelength excitation. The vibrational modes enhanced are generally totally symmetric and distort the molecule along directions of electron density changes between the ground and the resonant electronic excited state.[11] Preresonance excitation of derivatives such as sulfate, acetone, and ace-

0003-7028/88/4201-0083$2.00/0

tonitrile result in no observed enhancement by the expected valence transitions between 160 and 200 nm.[1,3] Indeed, the utilization of conventional preresonance Raman dispersion relationships to analyze the experimental data projects that far-UV transitions (<100 nm) will dominate the preresonance enhancement. In contrast, the ~180 nm $\pi \rightarrow \pi^*$ transitions of species such as nitrate,[3] acetamide, and *N*-methylacetamide[1] dominate the preresonance enhancement for both visible and UV (>220 nm) excitation of these molecules.

This pattern of preresonance intensity enhancement forced us, earlier, to question the existence in the condensed phase of discrete valence transitions for those species which have their first valence transition energies above, or comparable to, ionizing, Rydberg, or solvent-solute charge transfer bands.[1,3] Indeed, the existence of discrete valence transitions has recently been discussed theoretically, and the limitations of molecular orbital and valence bond descriptions of excited-state electronic structure have been noted.[27-30] Further, the basis sets which are required to correctly calculate Rydberg molecular excitations are only now beginning to be routinely utilized in quantum calculations.[27,28]

In this study we continue the examination of resonance enhancement in the simple molecules: water, imidazole (ImH), and imidazolium (ImH_2^+). The preresonance excitation profiles probe the excited-state structure. The preresonance excitation profiles of imidazole and imidazolium show the dominance of the first two $\pi \rightarrow \pi^*$ transitions between 180 and 220 nm—a result which is consistent with a recent report by Caswell and Spiro,[10] who measured the imidazole and imidazolium Raman intensities with excitations between 229 nm and 200 nm. We find the UV intensities are dominated by the 218-nm and 204-nm $\pi \rightarrow \pi^*$ transitions. We find no evidence for a contribution from the strong $\pi \rightarrow \pi^*$ transition at 190 nm in our preresonance Raman excitation profiles of imidazole and imidazolium. Our excitation profiles indicate that selective enhancements of the histidine imidazole sidechains of proteins require excitation near 200 nm.

EXPERIMENTAL

Imidazole (ImH) obtained from Aldrich Chemical Co. was vacuum sublimed before use. Na_2SO_4 was obtained from Merck and Co. The internal standard SO_4^{-2} concentration was 0.21 **M** for ImH solutions and 0.20 **M** for imidazolium (ImH_2^+) solutions. The ImH and ImH_2^+ concentrations used varied between 0.5 **M** and 0.003 **M**. The ImH_2^+ solutions (pH = 3.6 to 4.3) were prepared by the acidification of aqueous ImH solutions with 1 **M** HCl.

The laser beam was defocused in the sample to avoid nonlinear Raman processes, and to minimize the production of photochemical transients.[9] The sample solutions were pumped through a quartz capillary by the use of a peristaltic pump and were discarded after a single pass. The Raman intensities depended linearly on the incident laser power. Absorption spectra of the irradiated solutions were identical to those of the original, except for samples excited at 220 nm. These samples showed absorption decreases of ~15% at the 206-nm absorption band maxima, and new absorption features appeared at 265 nm. The Raman spectrometer used has been described in detail elsewhere.[31]

The monochromator throughput efficiency was determined by imaging light from a standard intensity lamp onto a Lambert surface prepared from Kodak white reflectance standard. The scattered light was imaged through the monochromator.

The total differential Raman cross sections of the analyte Raman bands were calculated from the expression:[1,3,5]

$$(\sigma_R)_A = (\sigma_R)_S \frac{I_A E(\nu_0 - \nu_S) C_S}{I_S E(\nu_0 - \nu_A) C_A} \quad (1)$$

where σ_A and σ_S are the total differential Raman cross sections of the analyte and the internal standard, respectively. The total differential Raman cross sections of SO_4^{-2} were taken from Dudik *et al.*[3] I_A and I_S are the total integrated intensities of the analyte and internal standard bands. $E(\nu_0 - \nu_A)$ and $E(\nu_0 - \nu_S)$ are the monochromator throughput efficiencies for the analyte and internal standard Raman bands, and C_A and C_S are the analyte and internal standard concentrations.

The total integrated intensity ratios between the imidazole bands and the 981-cm^{-1} SO_4^{-2} internal standard Raman band derived from peak height intensity measurements. We corrected the peak height ratios for differences in the bandwidth between the analyte and the SO_4^{-2} bands by accounting for the instrument transfer function to the Reticon pixel elements and by assuming Gaussian bandshapes.[32] The total differential Raman cross sections of the imidazolium bands and the 1645-cm^{-1} water band were determined directly from peak area measurements.

We estimate that the quoted cross sections are accurate to within ±20%. The major uncertainty derives from uncertainties in the cross-section values of sulfate.[3] Because the relative standard deviations of the excitation profile data are similar, each point should contribute equally to the excitation profile fit.

RESULTS

Figure 1 shows Raman spectra of ImH excited at 457.9, 310, 230, and 220 nm. The intense band at 981 cm^{-1} derives from a symmetric sulfate vibration, and the broad band at ~1645 cm^{-1} is due to an O-H bending vibration of H_2O. The normal mode assignments and potential energy distribution (PED) of the observed ImH vibrations are listed in Table IA.[33,34,35] The Raman bands observed below 1600 cm^{-1}, except for the 917-cm^{-1} band, derive mainly from in-plane C-C, C-N stretching and N-H and/or C-H deformations. The 917-cm^{-1} band is an out-of-plane ring deformation. Four intense polarized bands at 1160, 1260, 1328, and 1430 cm^{-1} dominate the ImH Raman spectra. The Raman differential cross sections of these bands increase together as the excitation wavelength decreases. In contrast, the relative intensities of the polarized 1135-cm^{-1} and depolarized 1065- and 1098-cm^{-1} bands decrease, and the relative intensity of the 930-cm^{-1} band increases as the excitation wavelength decreases.

Figure 2 shows the excitation frequency dependences of the total differential Raman cross sections, σ_A. The σ_A

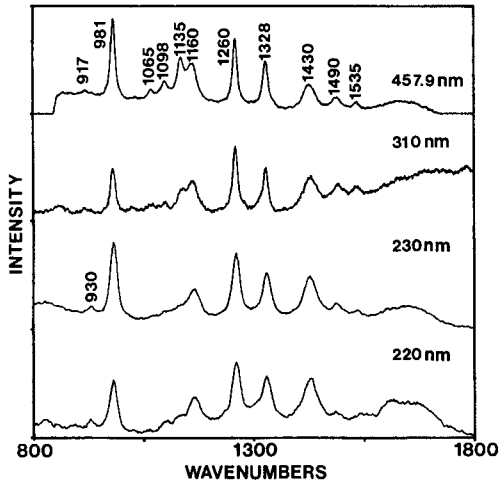

FIG. 1. Raman spectra of imidazole. The aqueous solutions are 0.21 M in Na_2SO_4. λ_{ex} = 457.9 nm: 0.48 M ImH; bandpass = 5.3 cm^{-1}; laser power = 100 mW; accumulation time = 1 s. λ_{ex} = 310.0 nm: 0.48 M ImH; bandpass = 7.3 cm^{-1}; pulses averaged = 12,000 (10 min scan). λ_{ex} = 230.0 nm: 12 mM ImH; bandpass = 13.2 cm^{-1}; pulses averaged = 24,000. λ_{ex} = 220.0 nm: 4.8 mM ImH; bandpass = 14.5 cm^{-1}; pulses averaged = 36,000. Laser pulse energy was less than 0.5 mJ/pulse.

values increase by ~10^4 as the excitation frequency increases from 19,000 cm^{-1} to 45,000 cm^{-1}. The solid lines are nonlinear least-square fits of the data to a modified Albrecht A-term expression:[1,3,5,36-38]

$$\sigma_A = K_1\nu_0(\nu_0 - \nu_A)^3\left(\frac{\nu_e^2 + \nu_0^2}{(\nu_e^2 - \nu_0^2)^2} + K_2\right)^2 \qquad (2)$$

where ν_0 is the excitation frequency, ν_A is the frequency of the vibrational mode, and ν_e is the transition frequency from the ground state to the preresonant excited electronic state. K_1 is a scaling parameter and K_2 is a constant that phenomenologically models contributions from states in the far-UV.

The ν_e, K_1, and K_2 values obtained from the nonlinear least-squares fits are shown in Table II. The electronic transition giving preresonance enhancement for each Raman band is extrapolated by the modified A-term to occur between 48,400 cm^{-1} and 49,100 cm^{-1} (204–207 nm); the absorption spectrum of ImH in aqueous solution shows absorption maxima at 48,500 cm^{-1} (206 nm) and 52,000 cm^{-1} (192 nm) which have been assigned to $\pi \rightarrow \pi^*$ transitions.[39-47]

The broken lines in Fig. 2 derive from nonlinear least-squares fits of the data to an unmodified A-term expression (Eq. 2, where $K_2 = 0$). These fits to an unmodified A-term are clearly unacceptable, and they result in ν_e values ranging between 54,400 and 59,300 cm^{-1}. Obviously, more than one $\pi \rightarrow \pi^*$ transition is required to describe the individual Raman cross-section excitation profiles of ImH. For excitation in the visible spectral region, the K_2 term dominates and the intensities derive mainly from states in the far-UV.[5] As the excitation frequency increases, the strongly allowed electronic transition or transitions at ~205 nm begin to dominate the preresonance enhancement.

Figure 3 shows the Raman spectra of ImH_2^+ excited at 514.5, 240, and 220 nm.The polarized 1215- and 1460-cm^{-1} bands dominate the ImH_2^+ Raman spectra, while

TABLE I. Normal mode assignments for imidazole and imidazolium.

A. Imidazole

Frequency (cm^{-1})	ρ[a]	Symmetry class	Assignment[b]	PED for stretching vibration[c] $\nu(N_3\text{-}C_2)$	$\nu(N_1\text{-}C_5\ N_3\text{-}C_4)$	$\nu(N_1\text{-}C_2)$	$\nu(C_4\text{-}C_5)$
917	dp	A″	ω(R)	14%	13%	—	—
930	?	?		—	19%	—	10%
1068	dp	A″	δ(R)	—	29%	18%	14%
1098	dp	A″	δ(R) + δ(C-H)	7%	25%	—	—
1135	p	A′	δ(R) + δ(C-H)	12%	9%	—	—
1160	p	A′	δ(R) + $\delta(N_1\text{-H})$	6%	—	—	—
1260	p	A′	δ(R) + $\delta(C_2\text{-H})$	12%	4%	4%	9%
1328	p	A′	δ(R)(ring breathing)	—	24%	33%	—
1430	p	A′	$\delta(N_1\text{-H})$	16%	—	—	23%
1490	p	A′	δ(R) + $\delta(C_2\text{-H})$	—	30%	18%	—
1535	p	A′	δ(R) + $\delta(N_1\text{-H})$	24%	19.5%	—	8%

B. Imidazolium[d]

Frequency (cm^{-1})	ρ[a]	Symmetry class	Assignment[b]
910	p	A_1	δ(R)
1068	—	B_1	δ(C-H)
1106	—	B_1	δ(C-H)
1135	p	A_1	δ(N-H)
1215	p	A_1	δ(R)(ring breathing)
1248	p	A_1	δ(C-H)
1412	—	B_1	δ(R)
1460	p	A_1	δ(R)

[a] p, polarized; dp, depolarized.
[b] ω = out-of-plane deformation; δ = in-plane deformation; ν = stretching.
[c] Potential energy distribution from Ref. 38.
[d] Polarization, symmetry class, and assignments are from Bellocq and Garrigou-LaGrange (Ref. 48).

bands at 981 and 1645 cm^{-1} are due to sulfate and H_2O, respectively. Table IB lists the vibrational assignments for the ImH_2^+ bands.[48] The 1215-cm^{-1} band is assigned as a ring breathing mode, while the 1460-cm^{-1} band is assigned to an in-plane ring deformation.

The total differential Raman cross-section excitation profiles for the 1215- and 1460-cm^{-1} bands of ImH_2^+ are shown in Fig. 4. The solid lines are fits to Eq. 2. The 220-nm cross sections of the ImH_2^+ bands are approximately three times that of ImH. The total differential Raman cross sections and the K_1, ν_e, and K_2 values are shown in Table III. More than one excited state is important for modeling the dispersion of the ImH_2^+ cross sections, since unacceptable fits result from Eq. 2 when $K_2 = 0$ (broken lines). The excited-state transition energy extrapolated from the modified A-term fit for the 1215- and 1460-cm^{-1} bands are 47,700 and 48,500 cm^{-1}, respectively. These values are close to the frequency of the first observed ImH_2^+ $\pi \rightarrow \pi^*$ electronic transition at 48,500 cm^{-1} (206 nm).[39]

The relative intensities of the ImH_2^+ bands at 910, 1068, 1106, and 1135 cm^{-1} decrease in comparison to the strong ImH_2^+ bands at 1215 and 1460 cm^{-1} as the excitation wavelength decreases. This indicates a smaller relative preresonance enhancement by the 206-nm transition for these modes, in comparison to the 1215- and 1460-cm^{-1} ImH_2^+ vibrations. The Raman spectrum excited at 220 nm clearly shows a high-frequency shoulder on the 1215-cm^{-1} band which may result from enhancement of the 1248-cm^{-1} ImH_2^+ band (Table IB). The in-

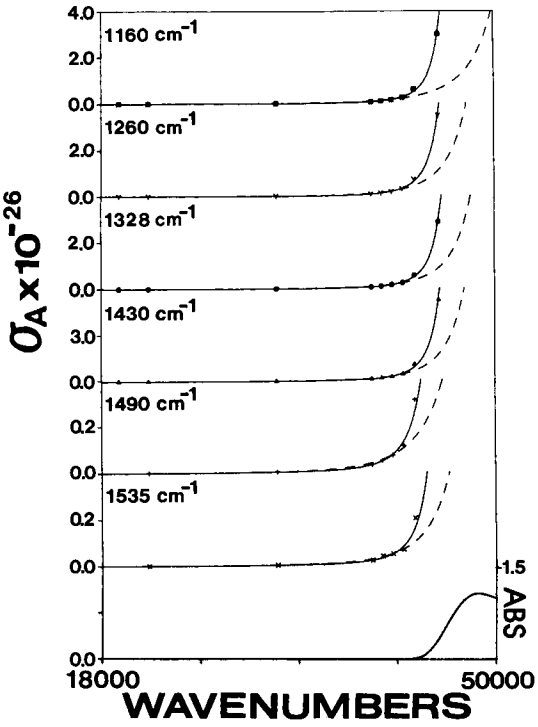

FIG. 2. Excitation profiles and the absorption spectrum of ImH. The total differential Raman cross sections are in units of cm²/(molc·str.). The solid curves derive from a nonlinear least-squares fit to a modified Albrecht A-term, while the broken lines are the nonlinear least-squares fits to Eq. 2, where $K_2 = 0$. The absorption spectrum is shown for a 0.22 mM ImH solution; pathlength = 1.0 cm.

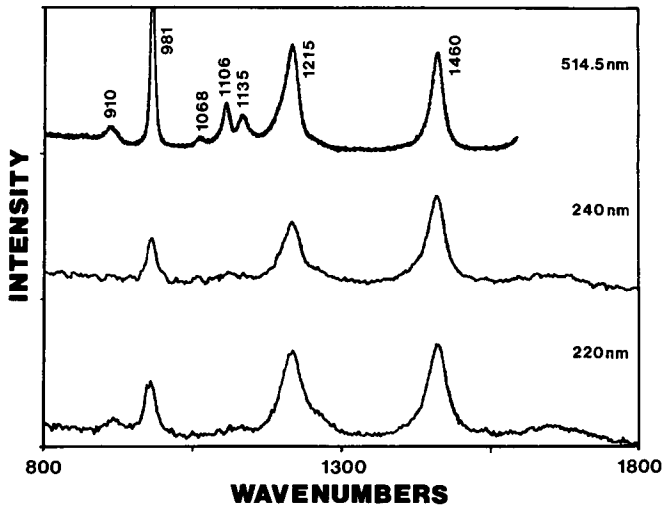

FIG. 3. Raman spectra of imidazolium. The aqueous solutions are 0.20 M in Na_2SO_4, λ_{ex} = 514.5 nm: 0.42 ImH_2^+; bandpass = 4.2 cm⁻¹; laser power = 80 mW; accumulation time = 1 s. λ_{ex} = 240.0 nm: 67 mM ImH_2^+; bandpass = 12.2 cm⁻¹; pulses averaged = 24,000. λ_{ex} = 220.0 nm: 2.7 mM ImH_2^+; bandpass = 14.5 cm⁻¹; pulses averaged = 36,000.

tensity of the 1215-cm⁻¹ band, relative to that of the 1460-cm⁻¹ band, decreases as the excitation wavelength decreases from 514.5 nm to 250 nm; however, excitation below 250 nm results in a relative intensity increase of the 1215-cm⁻¹ band.

In addition to the strong enhancement of the fundamental ImH and ImH_2^+ Raman bands, strong enhancements of the overtone and combination bands occur as the excitation wavelength approaches the ~200-nm absorption bands (Fig. 5). The most intense ImH combination band at 2590 cm⁻¹ derives from the 1260- and 1328-cm⁻¹ bands. The three ImH_2^+ overtone and combination bands derive from combinations of the 1215-cm⁻¹ band and the bands at 910, 1215, and 1460 cm⁻¹.

As seen in Fig. 1, the 1645-cm⁻¹ H_2O band intensity increases relative to that of the sulfate band as the excitation frequency increases. The cross sections for the 1645-cm⁻¹ H_2O vibration are tabulated in Table IV and its excitation profile is shown in Fig. 6. The solid and broken lines are fits to a modified ($K_2 \neq 0$) and unmodified Albrecht A-term ($K_2 = 0$), respectively. The preresonant excited state extrapolates to 147,000 cm⁻¹ (68 nm) from the unmodified A-term fit and to 60,400 cm⁻¹ (166 nm) from a modified A-term fit. In fact, the intensity of the water bending vibration increases only slightly faster than ν_0^4. Our measured value of 9×10^{-32} cm²/molc·str in condensed-phase water compares with a value of 3.3×10^{-32} cm²/molc·str for water vapor, as measured by Murphy[49] with 514.5-nm excitation. This difference may be partially accounted for by the local field[3] difference between the gas- and condensed-phase samples.

DISCUSSION

Preresonance enhancement of symmetric vibrations is expected to be dominated by A-term scattering in which the Raman vibrational transition is mediated through a geometric distortion of the resonant excited electronic state relative to the ground state. Indeed, previous studies of the symmetric vibrations of NO_3^-, *N*-methylacetamide, acetamide, benzene, toluene, and phenylalanine successfully modeled the preresonance excitation using Albrecht A-term expressions.[1,3,5,11] These studies demonstrated that the 180–210 nm $\pi \rightarrow \pi^*$ transitions of

TABLE II. Total differential Raman scattering cross sections[a] for imidazole and the K_1, ν_e, K_2 and parameters.

Frequency (cm⁻¹)	Total differential Raman cross section, $\sigma_A \times 10^{-26}$ Excitation (nm)							Modified A-term		
	514.5	457.9	310.0	250.0	240.0	230.0	220.0	$K_1 \times 10^{-30}$	ν_e cm⁻¹	$K_2 \times 10^{-9}$
1160	6.0×10^{-4}	1.1×10^{-3}	9.3×10^{-3}	0.075	0.16	0.62	3.0	3.62	44,800	3.12
1260	3.7×10^{-4}	6.9×10^{-4}	7.6×10^{-3}	0.081	0.18	0.71	3.5	6.00	49,100	1.67
1328	3.1×10^{-4}	5.7×10^{-4}	6.1×10^{-3}	0.066	0.16	0.56	2.9	4.75	49,100	1.73
1430	5.4×10^{-4}	9.0×10^{-4}	0.010	0.12	0.27	1.1	5.2	9.10	49,100	1.58
1490	—	3.2×10^{-4}	3.6×10^{-3}	0.034	0.074	0.31	—	1.48	48,400	2.75
1535	—	2.0×10^{-4}	1.8×10^{-3}	0.020	0.048	0.20	—	0.93	48,400	2.64

[a] The total differential Raman scattering cross section in units of cm²/(molc·steradian).

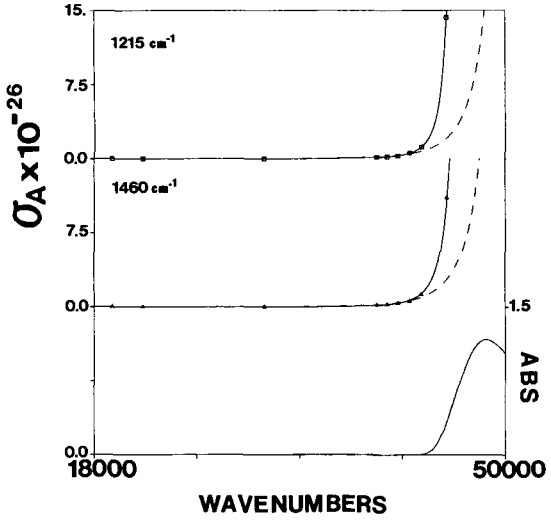

FIG. 4. Excitation profiles and absorption spectrum of ImH_2^+. The total differential Raman cross sections are in units of $cm^2/(molc \cdot str.)$. The solid curves derive from a nonlinear least-squares fit to a modified Albrecht A-term, while the broken lines are nonlinear least-squares fits to Eq. 2, where $K_2 = 0$. The absorption spectrum is shown for 0.22 mM ImH_2^+ in dilute HCl solution; pathlength = 1.0 cm.

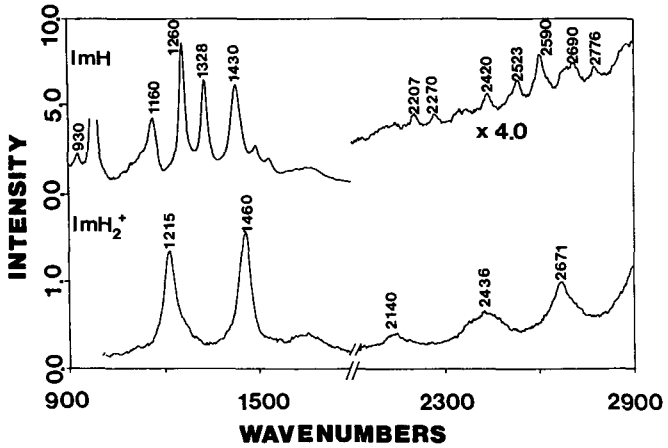

FIG. 5. Raman spectra of ImH excited at 230 nm and ImH_2^+ excited at 220 nm. ImH: bandpass = 13.2 cm^{-1}; pulses averaged = 24,000. ImH_2^+: bandpass = 14.5 cm^{-1}; pulses averaged = 36,000. Laser pulse energy was less than 0.5 mJ/pulse.

these compounds dominate their preresonance Raman intensities. The normal A-term expression (Eq. 2 when $K_2 = 0$) will accurately model the preresonance enhancement if:

1. One excited state dominates the enhancement.
2. The homogeneous linewidth of the transition is small in comparison to the frequency offset from resonance.
3. The displacement of the resonant excited state relative to the ground state is small so that the first few terms of the Franck-Condon sum dominates.

The approximations required for accurate modeling of the preresonance enhancement must fail as excitation occurs farther in the UV. Indeed, as excitation approaches the L_a transition in phenylalanine, the Albrecht A-term overestimates the intensities because it ignores the homogeneous linewidth or damping factor for the transition.[11] The unmodified A-term expression fails for those vibrational modes of acetamide and *N*-methylacetamide which contain significant amounts of C-C stretching, because additional electronic transitions that are farther into the UV than is the 180 nm $\pi \rightarrow \pi^*$ transition also strongly contribute to preresonance enhancement;[1] the K_2 term is required for adequate modeling of the preresonance Raman excitation profile data. For benzene excited in the *visible* spectral region, the K_2 term completely dominates the preresonance enhancement.[5]

Other phenomena may occur to make preresonance Raman enhancement depart from A-term-like behavior. For example, a resonant valence transition may occur at an energy which overlaps that of ionizing transitions, Rydberg transitions, and solute-solvent charge transfer transitions. These transitions would strongly mix and give broad transitions with large homogeneous linewidths. The very existence of discrete valence transitions within the "sea" of ionizing and Rydberg transitions is questionable, especially in the condensed phase.[30]

The magnitude of the Franck-Condon enhancement of a vibrational normal mode is proportional to the square of the geometric distortion between the ground and excited state of the molecule along a coordinate parallel to the normal mode vibrational coordinate. In the case of a valence transition, distortion of the molecule along a symmetric normal mode coordinate will lead directly to Raman enhancement. In an ionizing or Rydberg transition, an electron is promoted from a valence orbital out of the molecule, or to a very diffuse orbital. This response is expected to result in a smaller distortion of the molecular geometry of the excited state than generally occurs in a valence transition; the promoted electron either leaves the system or fills a nonbonding orbital, rather than filling an antibonding orbital. Thus, Rydberg and ionizing transitions should be weaker sources of resonance Raman enhancement than are valence transitions.

Extensive mixing between valence, Rydberg, and ionizing electronic transitions may be responsible for the broad diffuse absorption bands commonly observed in vacuum UV absorption studies. For Raman scattering this mixing will be reflected in a large damping factor in the resonance expression denominator. The dispersion of the Raman cross section as resonance is approached

TABLE III. Total differential Raman scattering cross sections[a] for imidazolium and the K_1, ν_e, and K_2 parameters.

Frequency (cm^{-1})	Total differential Raman cross section, $\sigma_A \times 10^{-26}$ Excitation (nm)						Modified A-term		
	514.5	457.9	320.0	250.0	230.0	220.0	$K_1 \times 10^{-30}$	ν_e cm^{-1}	$K_2 \times 10^{-9}$
1215	1.1×10^{-3}	1.8×10^{-3}	8.1×10^{-3}	0.16	1.2	14	3.62	47,700	3.93
1460	8.2×10^{-4}	1.4×10^{-3}	9.6×10^{-3}	0.23	1.3	11	8.64	48,500	2.13

[a] The total differential Raman scattering cross section in units of $cm^2/(molc \cdot steradian)$.

TABLE IV. Total differential Raman scattering cross sections[a] of the 1645 cm^{-1} vibration of water and the ν_e, K_1, and K_2 parameters.

H_2O band (cm^{-1})	Total differential Raman cross section, $\sigma_A \times 10^{-30}$ Excitation (nm) 457.9	280.0	250.0	235.0	225.0	220.0	A-term ($K_2 = 0$) $K_1 \times 10^{-29}$	ν_e cm^{-1}	Modified A-term $K_1 \times 10^{-32}$	ν_e cm^{-1}	$K_2 \times 10^{-9}$
1645	0.09	0.7	1.2	2.0	2.4	2.6	17	147,000	0.89	60,400	6.72

[a] The total differential Raman scattering cross section in units of $cm^2/(molc \cdot steradian)$.

would decrease due to the large damping factor. Attempts to fit the resulting Raman intensity dependence with an A-term expression would overestimate the value of the preresonant transition energy. These phenomena could be responsible for the high transition energies found for the A-term fits of the preresonance Raman excitation profiles of the symmetric vibrations of CH_3CN, SO_4^{2-}, and ClO_4^- as well as for the ImH and ImH_2^+ and water data presented here.[3]

Modeling of the excitation profiles with the modified Albrecht A-term utilizes the K_2 parameter to account for the near constant contribution of the high-energy states (whether diffuse or not). For both ImH and ImH_2^+, the K_2 term dominates the enhancement for the excitation in the visible and near-UV spectral regions; however, as excitation occurs farther into the UV, the Raman intensity becomes dominated by the strong $\pi \rightarrow \pi^*$ transitions between 200 and 220 nm. Our data suggest that a transition (or transitions) around 49,100 cm^{-1} (204 nm) dominates the UV enhancement. This result agrees with the recent 200–230 nm excitation profile data of Caswell and Spiro,[10] who appear to have resolved two separate $\pi \rightarrow \pi^*$ transitions for both ImH and ImH_2^+ between 200 and 220 nm. We cannot separately resolve the contribution of these two transitions; the extrapolated transition energy from the modified A-term occurs at an intermediate energy.

For ImH the two transitions at ~204 and 218 nm assigned by Caswell and Spiro appear to contribute with the same sign to the value of the Raman polarizability, as does the far-UV transition which dominates with visible wavelength excitation. This is evident because the cross sections of the bands monotonically increase at a rate faster than that given by a ν^4 dependence. In contrast, the ImH_2^+ band at 1215 cm^{-1} shows evidence of destructive interference between the two $\pi \rightarrow \pi^*$ transitions and the transition farther into the UV. The relative intensity of the 1215-cm^{-1} band decreases as the excitation wavelength decreases from 457.9 nm to 250 nm and then increases rapidly with shorter wavelength excitation. Indeed, the cross-section increase between 457.9 and 250 nm is less than that expected from a ν^4 dependence.

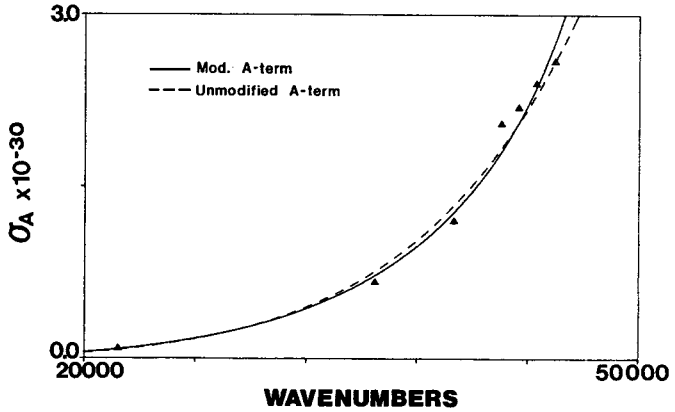

FIG. 6. Total differential Raman cross section excitation profile of the 1645-cm^{-1} H_2O band. The cross section is given in units of $cm^2/(molc \cdot str.)$. The solid line is a fit to Eq. 2, while the broken line is a fit to an unmodified A-term (Eq. 2, where $K_2 = 0$).

Although the 190-nm transition should also strongly contribute to resonance enhancement for ImH and ImH_2^+, we see no direct evidence for its contribution. We plan to extend our quantitative UV excitation profiles farther into the UV to resolve the contribution and assignment of this transition. It is obvious that the assignment of this transition will be interesting, since the earlier assignments seem to conflict with the recent Raman excitation data of Caswell and Spiro.[10]

The preresonance excitation profile of water is equally well modeled by a simple A-term or modified A-term expression, which yields either 147,000 (68 nm) or 60,400 cm^{-1} (166 nm), respectively, for the preresonant excited state energy. The K_2 term completely dominates the Raman intensities for the modified A-term fit and is responsible for almost all of the observed intensities. Indeed, the Raman cross section almost increases with a ν^4 dependence.

The vacuum UV absorption spectrum of water vapor shows a broad, relatively weak absorption at 60,000 cm^{-1} and the onset of an intense absorption continuum starting at 70,000 cm^{-1}, which continues to at least 160,000 cm^{-1}.[30] Fine structure is evident in the vapor-phase absorption spectrum above 70,000 cm^{-1}. The absorption spectra of ice and liquid water show some similarities to the vapor in band positions, but the bands are more diffuse and all fine structure disappears.[30] The modern interpretation of the optical transitions of water in the gas phase[30] suggests that they are mixtures of Rydberg and valence transitions. It is likely that the valence transitions of liquid water will be even more mixed and will include contributions of charge transfer transitions. Thus, the vacuum UV transitions of water will presumably be best described as collective excitations rather than molecular transitions. We conclude that the high preresonance energy extrapolated from the A-term fit for water derives from the lack of any discrete strong valence transitions in the UV. Possibly, the modified A-term fit transition energy is indicative of a weak enhancement of the water bending vibration by a liquid-phase absorption band which derives from the isolated 60,000 cm^{-1} water vapor absorption. The other water transitions are extensively broadened with linewidths comparable to the excitation frequency offset from resonance. Strong mixing of an excited state that gives intense preresonance enhancement into a continuum of states that are weaker sources of preresonance enhancement will result in a decreased dispersion of the preresonance intensities. We

can model the preresonance behavior by spreading the excitation over the bandwidth of the other transitions.

The Kramer-Heisenberg expression for Raman intensity indicates that, for one preresonant transition, the relationship between the Raman cross section and the Raman polarizability is given by:

$$\sigma_A \simeq \nu_0(\nu_0 - \nu_A)^3|\alpha|^2$$
$$= \nu_0(\nu_0 - \nu_A)^3\left(\frac{M^2}{\nu_e - \nu_0 - i\Gamma}\right)^2 \quad (3)$$

where M is the transition moment to the resonant excited state and Γ is the homogeneous linewidth; we have neglected the nonresonant term. Far from resonance, one can use appropriate approximations to derive the classical A-term expression. However, if the transition is spread over (mixed) with numerous other nonpreresonant Raman active transitions at similar frequencies, we can approximate the dispersion by integrating over the spectral interval over which the transition is spread (between ν_A and ν_B). Assuming that the transition is democratically spread over this interval, and that we can treat the intensity contribution at the modulus squared level, and that Γ is negligible in comparison to the offset from resonance:

$$|\alpha|^2 = \left[\frac{M^2}{\nu_b - \nu_a}\int_{\nu_a}^{\nu_b}\left(\frac{1}{\nu_e - \nu_0} + \frac{1}{\nu_e + \nu_0}\right)d\nu_e\right]^2$$
$$= \frac{2M^4}{(\nu_b - \nu_a)^2}\ln\frac{(\nu_b^2 - \nu_0^2)}{(\nu_a^2 - \nu_0^2)}. \quad (4)$$

The consequence of spreading the transition over a frequency range is a Raman cross section with less dispersion than that prescribed by the A-term. Attempts to use the A-term expression will result in artifactually high transition frequencies. This mixing between transitions is similar to increasing the value of Γ, which obviously decreases the dispersion of the Raman cross section. These phenomena may be responsible for the 147,000-cm^{-1} preresonance fit for water, and for the dominance of the K_2 terms of the modified A-term for excitation in the visible spectral region for imidazole and imidazolium, and for the far-UV preresonance transitions found for acetonitrile, SO_4^{2-}, and ClO_4^- and acetone.[1,3]

CONCLUSIONS

ImH and ImH_2^+ vibrations show large enhancements as excitation approaches resonance with the 190–220 nm $\pi \rightarrow \pi^*$ transitions. These transitions may prove useful for selectively exciting histidine residues in proteins; however, as pointed out by Caswell and Sprio,[10] significant interferences are likely to occur from phenylalanine and amide residues. The cross sections for the 1645-cm^{-1} vibration of H_2O have been determined, and this band can now be used as an internal intensity standard for Raman studies of aqueous solutions. Strong mixing of valence transfer, ionizing, and Rydberg transitions may account for the high-energy preresonance transitions found from fits of preresonance excitation profiles to Raman A-term expressions.

ACKNOWLEDGMENTS

We gratefully acknowledge Craig R. Johnson and Colleen Jones for helpful discussions. We also gratefully acknowledge support of this work from NIH Grant 1R01 GM30741-05. Sanford A. Asher is an Established Investigator of the American Heart Association; this work was completed during the tenure of an Established Investigatorship of the American Heart Association, Pennsylvania affiliate.

1. J. M. Dudik, C. R. Johnson, and S. A. Asher, J. Phys. Chem. **89,** 3805 (1985).
2. L. C. Mayne, L. D. Ziegler, and B. Hudson, J. Phys. Chem. **89,** 3395 (1985).
3. J. M. Dudik, C. R. Johnson, and S. A. Asher, J. Chem. Phys. **82,** 1732 (1985).
4. L. D. Ziegler and B. Hudson, J. Phys. Chem. **74,** 982 (1981).
5. S. A. Asher and C. R. Johnson, J. Phys. Chem. **89,** 1375 (1985).
6. D. P. Gerrity, L. D. Ziegler, P. B. Kelly, R. A. Desiderio, and B. Hudson, J. Chem. Phys. **83,** 3209 (1985).
7. L. D. Ziegler and A. C. Albrecht, J. Chem. Phys. **67,** 2753 (1977).
8. L. D. Ziegler and B. S. Hudson, J. Chem. Phys. **79,** 1134 (1983).
9. C. R. Johnson, M. Ludwig, and S. A. Asher, J. Am. Chem. Soc. **108,** 905 (1986).
10. D. Caswell and T. G. Spiro, J. Am. Chem. Soc. **108,** 6470 (1986).
11. S. A. Asher, M. Ludwig, and C. R. Johnson, J. Am. Chem. Soc. **108,** 3186 (1986).
12. L. Chinsky, B. Jolles, A. Laigle, and P.-Y. Turpin, J. Raman Spectrosc. **16,** 235 (1985).
13. R. P. Rava and T. G. Spiro, J. Am. Chem. Soc. **106,** 4062 (1984).
14. R. P. Rava and T. G. Spiro, J. Phys. Chem. **89,** 1856 (1985).
15. C. R. Johnson, M. Ludwig, S. E. O'Donnell, and S. A. Asher, J. Am. Chem. Soc. **106,** 5008 (1984).
16. W. L. Kubasek, B. Hudson, and W. L. Peticolas, Proc. Natl. Acad. Sci. (U.S.A.) **82,** 2369 (1985).
17. L. D. Ziegler, B. S. Hudson, D. P. Strommen, and W. L. Peticolas, Biopolymers **23,** 2067 (1984).
18. S. P. A. Fodor, R. P. Rava, T. R. Hays, and T. G. Spiro, J. Am. Chem. Soc. **107,** 1520 (1985).
19. S. Nocentini and L. Chinsky, J. Raman Spectrosc. **14,** 9 (1983).
20. R. A. Copeland, S. Dasgupta, and T. G. Spiro, J. Am. Chem. Soc. **107,** 3370 (1985).
21. R. A. Copeland and T. G. Spiro, Biochemistry **24,** 4960 (1985).
22. R. P. Rava and T. G. Spiro, Biochemistry **24,** 1861 (1985).
23. C. R. Johnson and S. A. Asher, Anal. Chem. **56,** 2258 (1984).
24. S. A. Asher, Anal. Chem. **56,** 720 (1984).
25. S. A. Asher and C. M. Jones, *New Applications of Analytical Techniques to Fossil Fuels,* ACS Symposium Series, M. Perry and H. Retcofsky, Eds. Am. Chem. Soc. Div. Fuel Chem. preprints **31,** 170 (1986).
26. C. M. Jones, T. A. Naim, M. Ludwig, J. Murtaugh, P. L. Flaugh, J. M. Dudik, C. R. Johnson, and S. A. Asher, Trends Anal. Chem. **4,** 75 (1985).
27. R. L. Whetten, S. G. Grubb, C. E. Otis, A. C. Albrecht, and E. R. Grant, J. Chem. Phys. **82,** 1115 (1985).
28. R. Roberge and D. R. Salahub, J. Chem. Phys. **70,** 1177 (1979).
29. R. S. Mulliken, Chem. Phys. Lett. **46,** 197 (1977).
30. M. B. Robin, *Higher Excited States of Polyatomic Molecules* (Academic Press, New York, 1985), Vol. III, Chap. VII and references therein.
31. S. A. Asher, C. R. Johnson, and J. Murtaugh, Rev. Sci. Instrum. **54,** 1657 (1983).
32. J. Murtaugh, Ph.D. Thesis, University of Pittsburgh, Pittsburgh (1987).
33. L. Columbo, P. Bleckman, B. Schrader, R. Schneider, and Th. Plesser, J. Chem. Phys. **61,** 3270 (1974).
34. S. Salama and T. G. Spiro, J. Am. Chem. Soc. **100,** 1105 (1978).
35. C. M. Jones, C. R. Johnson, S. A. Asher, and R. E. Shepherd, J. Am. Chem. Soc. **107,** 3772 (1985).
36. J. Tang and A. C. Albrecht, in *Raman Spectroscopy, Theory and Practice,* H. A. Szymanski, Ed. (Plenum Press, New York, 1970), Vol II., p. 33.
37. A. C. Albrecht and M. C. Hutley, J. Chem. Phys. **55,** 4438 (1971).
38. A. C. Albrecht, J. Chem. Phys. **34,** 476 (1961).
39. P. E. Grebow and T. M. Hooker, Biopolymers **14,** 871 (1975).
40. T. G. Fawcett, E. E. Bernaducci, K. Krogh-Jespersen, and H. J. Schugar, J. Am. Chem. Soc. **102,** 2598 (1980).

41. S. Cradock, R. H. Findlay, and M. H. Palmer, Tetrahedron **29**, 2173 (1973).
42. T. K. Ha, J. Mol. Struct. **51**, 87 (1979).
43. I. Fischer-Hjalmars and J. Nag-Chaudhuri, Acta Chem. Scand. **23**, 2963 (1969).
44. M. Sundbom, Acta Chem. Scand. **25**, 487 (1971).
45. R. W. Wagner, P. Hockman, and M. A. El-Bayoumi, J. Mol. Spectrosc. **54**, 167 (1975).
46. J. Del Bene and H. H. Jaffe, J. Chem. Phys. **48**, 4050 (1968).
47. C. M. Yoshida, T. B. Freedman, and T. M. Loehr, J. Am. Chem. Soc. **97**, 1028 (1975).
48. A.-M. Bellocq and C. Garrigou-LaGrange, Spectrochim. Acta **27A**, 1091 (1971).
49. W. F. Murphy, Mol. Phys. **33**, 1701 (1977).

Mathematical Justification of the Use of IR Transmission Spectroscopy for the Quantitative Analysis of Surface-Treated Powders

ANDERS HANNING*
Laboratory of Polymer Technology, University of Åbo Akademi, Porthansgatan 3, SF-20500 Åbo, Finland

Measuring the IR transmission through a loosely packed powder layer offers a cheap and experimentally simple method for the quantitative and qualitative analysis of surface-treated powders. It is, however, practically impossible to obtain a perfectly smooth and even powder layer—a fact that introduces large errors in the quantitative determination. To cope with this problem, one derives an equation, by means of which it is possible to carry out the determination irrespective of the layer-thickness variations. The equation is based on the use of an "internal thickness standard." The theory is illustrated with, and supported by, a series of determinations of a silane coupling agent on a phlogopite powder. As predicted by the theory, a linear relationship is obtained when the absorbance ratio of the silane and the standard is plotted against the relative amount of silane. The quantification limit of the method lies in the monolayer range, depending on the powder surface area and the specific silane absorptivity. The method is thought to work equally well with powder mixtures.

Index Headings: **IR Transmission spectroscopy; Powder analysis; Surface-treated powder; Aminosilane coupling agent.**

INTRODUCTION

IR spectroscopy is a well-established method for the qualitative and quantitative analysis of powders, powder mixtures, and surface-treated powders. Several sample preparation techniques exist. The method of choice is most often diffuse reflection spectroscopy (DRIFT), which has manifested itself as a convenient and fast method. The main drawback of this method is that the signal is not linearly related to the concentration of analyte, but has to be recalculated according to the Kubelka-Munk theory.[1,2] Other drawbacks are the necessity to use a specially designed, expensive sample cell, and the sensitivity to microgeometry and orientation effects.[2,3]

Internal reflection spectroscopy (MIR or ATR) has also been used. The problem in this case is to obtain a reproducible pressure and contact area between the powder and the crystal. Neither form of this method gives a straight line plot of signal against concentration, and careful calibration has to be carried out.

Conventional transmission techniques usually do not work out well. Mineral oil suspensions, of course, give rise to severe spectral interferences and, in the case of surface-treated powders, possibly to chemical interferences as well. The KBr pellet technique involves tremendous pressures, which could seriously affect the sample, especially in the case of surface-treated powders (e.g., coupling agents on mineral fillers for plastic composites). Besides, the intimate contact with the hygroscopic KBr could possibly give chemical interferences. The preparation of neat powder pellets (without KBr) is experimentally difficult, involves high pressures, and gives rise to light scattering problems.

Even though diffuse reflectance is the workhorse method for powder analysis, an experimentally simple and cheap method that gives a linear relationship between signal and concentration would offer an interesting alternative. Such an alternative is transmission through a loosely packed layer: a thin, loosely packed layer of powder is placed between two IR-transparent crystals, and a spectrum is run in the transmission mode. This method has one inherent weakness, namely the impracticality of obtaining an ideally smooth, even, and reproducible powder layer. This is a serious problem, giving rise to bad reproducibility and large quantitative errors, but it can be dealt with. A mathematical analysis shows that the use of an internal thickness standard will give passable accuracy for most purposes. The mathematical treatment is further depicted in the next section.

The present method was developed for the purpose of analyzing surface-treated powders, specifically quantification of silane coupling agents on mineral fillers for plastic composites. IR spectroscopy as a means of quantifying silane coupling agents on fillers has been used before. Ishida and Koenig used the transmission KBr technique.[4] Culler *et al.* used a technique similar to the

Received 20 February 1987; revision received 12 July 1987.
* Present address: Department of Analytical Chemistry, The Royal Institute of Technology, S-10044 Stockholm, Sweden.

0003-7028/88/4201-0090$2.00/0